

# Chapter 3

## Innovative Techniques for the Characterization of the Morphology, Geometry and Hydrological Features of Slow-Moving Landslides

**Ulrich Kniess, Julien Travelletti, Alexander Daehne, Dominika Krzeminska, Grégory Bièvre, Denis Jongmans, Alessandro Corsini, Thom Bogaard, and Jean-Philippe Malet**

**Abstract** In the last 10 years, landslide characterization has benefited from numerous developments in remote sensing, near surface geophysics, instrumentation and data processing. This section highlights various advances and innovative techniques or processing methods to characterize the morphology, structure and hydrological features of landslides. Airborne Laser Scanner (ALS) technique has emerged as a promising tool for characterizing slope morphology, with the perspective of automatic detection of landslide-affected areas. Combining ALS-data DTM with geophysical and geotechnical information has allowed to reconstruct the 3D landslide geometry considering data uncertainty and resolution. This is a significant forward step in landslide investigation. Of major importance is also

---

U. Kniess • G. Bièvre • D. Jongmans (✉)  
Institut des Sciences de la Terre, CNRS UMR 5275, Observatoire des Sciences de l'Univers,  
Université Joseph Fourier, BP 53, FR-38041, Grenoble Cedex 09, France  
e-mail: [denis.jongmans@ujf-grenoble.fr](mailto:denis.jongmans@ujf-grenoble.fr)

J. Travelletti • J.-P. Malet  
Institut de Physique du Globe de Strasbourg, CNRS UMR 7516, Université de Strasbourg/EOST,  
5 rue René Descartes, F-67084 Strasbourg Cedex, France

BEG, Bureau d'Etudes Géologiques SA, Rue de la Printse 4, CH-1994 Aproz, Switzerland

A. Daehne • A. Corsini  
Department of Earth Sciences, University of Modena and Reggio Emilia University,  
Largo Sant' Eufemia 19, IT-41100 Modena, Italy

Department of Geosciences, University of Missouri – Kansas City, 5110 Rockhill Road,  
Kansas City, MO 64110, USA

D. Krzeminska • T. Bogaard  
Water Resources Section, Faculty of Civil Engineering and Geosciences, Delft University  
of Technology, Stevinweg 1, 2628 CN Delft, The Netherlands

the detection and monitoring of water infiltration in the sliding masses, using indirect prospecting techniques such as ERT and distributed temperature sensing (DTS) using fibre-optic cables. These new techniques could be a major help in understanding the water paths and in designing appropriate remediation systems. Finally, although most of these results have been obtained in clayey landslides, the applied methods can be extended to other landslide types, with some technical adaptations.

## Abbreviations

ALS	Airborne Laser Scanner
DEM	Digital Elevation Model
DTM	Digital Terrain Model
ERT	Electrical Resistivity Tomography
RMSE	Root Mean Square Error
DGPS	Differential Global Positioning System
DTS	Distributed Temperature Sensing
GPR	Ground Penetrating Radar

## 3.1 Introduction

During the last decade, techniques for landslide investigation and monitoring have undergone rapid development. Innovative methods include remote sensing imaging of the surface, geophysical imaging of the landslide structures and easy-to-deploy point measurements in the landslide mass. This section discusses advanced methods to characterize the morphology of areas affected by active landslides from the processing of airborne laser scanner point clouds (ALS). In particular, the possibility to automatically distinguish sliding zones from stable areas is discussed by characterizing the terrain roughness. Shallow geophysical prospecting has also considerably evolved with the emergence of 3D spatial imaging and 4D time and space imaging, allowing the spatial and temporal variations of landslides to be determined (Jongmans and Garambois 2007). The combination of remote sensing methods and near surface geophysical techniques offers the possibility to image the landslide surface and the structure at depth. ALS data and seismic noise measurements have been used to investigate the 3D geological structure below two large clayey landslides in the Trièves Plateau (France). It is shown that the bedrock topography had, and still has, a major influence on the kinematics of the two landslides. Because multi-source data have different spatial resolution and characteristics, data interpretation and integration for building a 3D geometrical model can turn out to be a difficult task (Bichler et al. 2004; Caumon et al. 2009).

A new methodology for building 3D structure has been proposed for landslides exhibiting a continuous basal shear surface. Finally, rainfall and its consequences (erosion, infiltration, water level rise, pore water pressure built up) have a major influence on the triggering or reactivation of mass movements in clay slopes. The relation between rainfall, water infiltration and sliding activity is however complex, and innovative field investigation is necessary to understand how water infiltrates in cohesive material. The section discusses an attempt to monitor water infiltration and subsurface flow within a clay-shale landslide using time-lapse electrical resistivity tomography (ERT). This electrical survey took place during an artificial rainfall experiment at the Laval landslide (South French Alps). An alternative for soil moisture monitoring is to perform high-resolution temperature measurements using fiber-optic cable. Temperature is used as a tracer to detect spatial and temporal variation in soil moisture conditions through the monitoring of soil thermal properties. The geological, morphological and kinematic settings of the main landslides quoted in this paper – Avignonet and Harmalière (Trièves Plateau, France), Super-Sauze (Barcelonette basin, France), Laval (Draix, France) and Valoria (Northern Apennines, Italy), can be found in Bièvre et al. (2011, 2012), Malet et al. (2003), Travelletti and Malet (2012) and Daehne (2011).

## 3.2 Characterization of Landslide Morphology from ALS Data Processing

### 3.2.1 Influence of Vegetation Filtering

In order to obtain a DTM (Digital Terrain Model or bare earth model), which will hold the relevant geomorphological information on a landslide, every point in the point-cloud has to be classified (e.g. as ground, building, low/mid/high vegetation), assigning a tag with the reflecting material to every cloud point. Many filtering methods have been proposed to filter vegetation (Sithole and Vosselman 2001; Zhang and Whitman 2005). For the Trièves Plateau (Avignonet and Harmalière landslides), a “Hierarchical robust filtering” method (Briese et al. 2002) has been applied to such highly vegetated slopes, as shown by the comparison between unfiltered and filtered 2006 ALS point-clouds at Avignonet (Fig. 3.1). In order to derive an equally spaced bare-earth DTM for further morphological analysis, the ALS point cloud at Avignonet and Harmalière landslides was classified and filtered using ‘Hierarchical robust filtering’ with the software SCOP++. The average density for both scans is therefore about 3 pts·m<sup>-2</sup>. The comparison of the point cloud densities before and after the filtering (Fig. 3.1) shows that the decrease is higher in vegetated areas.

In order to evaluate the quality of the vegetation filtering, two test-areas of 100 × 100 m characterized by rough terrains are filtered manually using

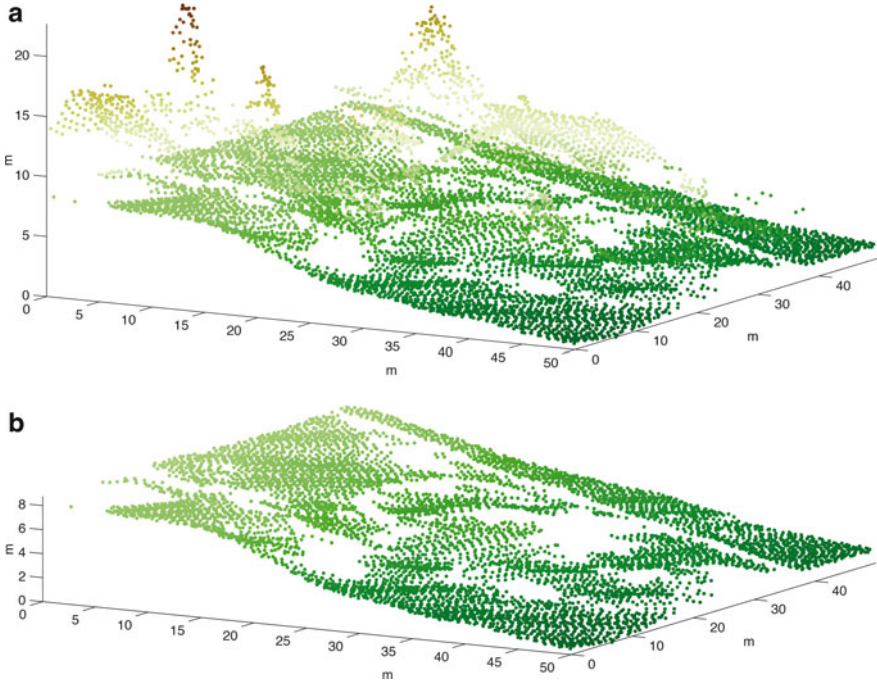


**Fig. 3.1** Vegetation filtering on a data subset of the 2006 ALS point-cloud showing the unfiltered (a) and filtered point-cloud (b). The unfiltered raw point-cloud also includes points resulting from reflections on houses and trees, whereas the filtered point-cloud contains only the points classified as ground

a 3D-Viewer for point clouds with some advanced point selection tools Point Cloud Mapper (PCM). Figure 3.2a shows the unfiltered and filtered DEM (Digital Elevation Model) with the location of the two test-areas. The manual filtered point-cloud and the automatic filtered point-cloud are gridded ( $2 \times 2$  m) and the difference is shown in Fig. 3.2b. Test-area 1 is situated in dense forest with steep slopes ( $>25^\circ$ ) including a drainage channel. Automatic filtering seems to throw out too many points of the bare-earth as the DTM is too low in average ( $-0.85$  m). The maximal errors are about 3 m and the standard deviation of 0.70 m shows a quite high variation. The second test-area is located in a village on just a minor slope ( $<10^\circ$ ) including some houses and trees. Results from the automatic filtering are better than for test-area 1, but still below the reference in average ( $-0.34$  m). The standard deviation of 0.37 m indicates that the maximal errors of  $-2.41$  and 1.01 m are mainly outliers. The graphical representation of the two areas (Fig. 3.2b) shows that main difficulties are connected with lineaments, the drainage channel in test-area 1 and tree/bush-chains in test-area 2. These two test-areas are extreme cases and more isolated houses or/and trees have been filtered with less error.

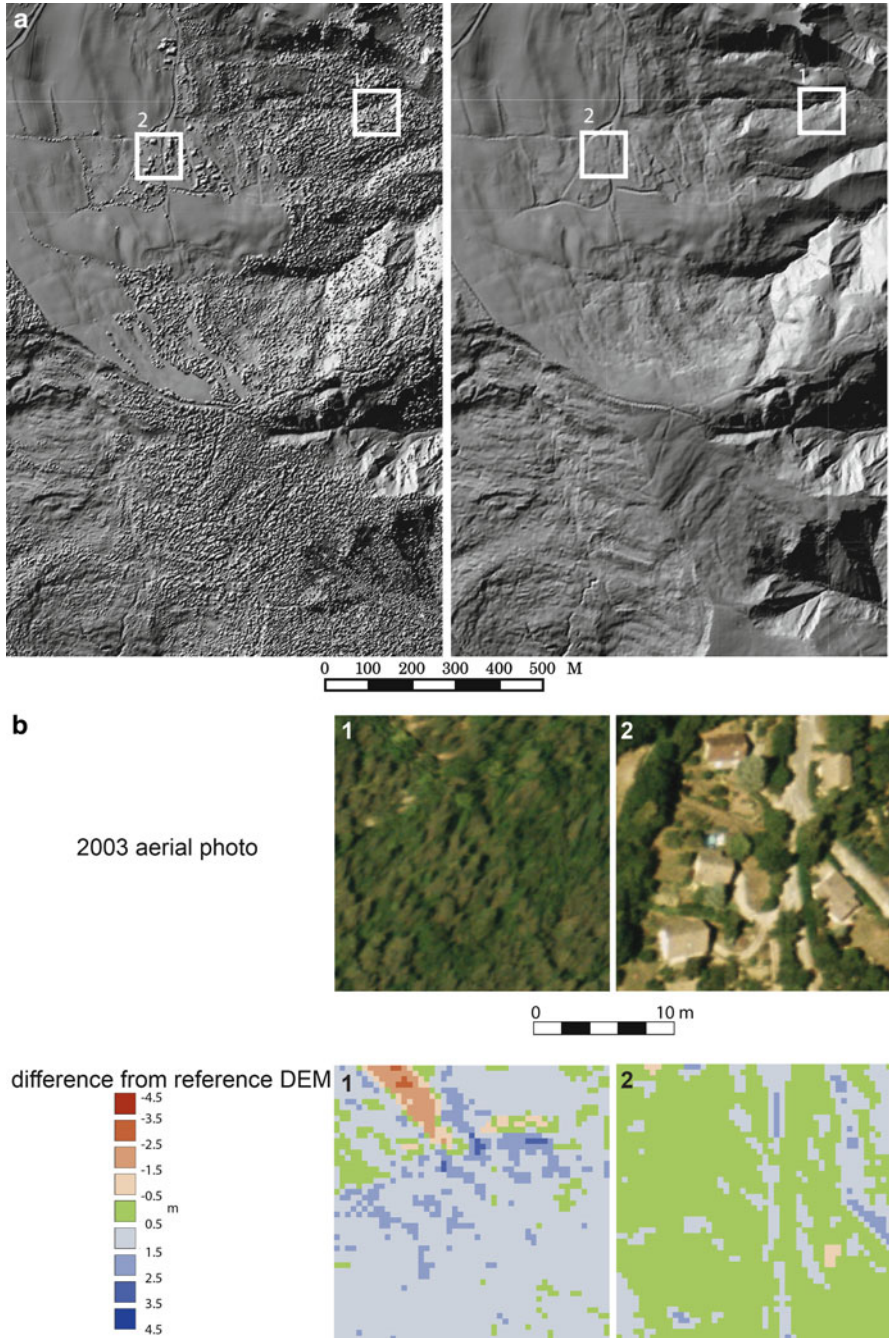


**Fig. 3.2** Analysis of the upper part of Harmalière landslide. (a) Comparison between the shaded reliefs from the unfiltered (*left*) and filtered (*right*) DEMs, (b) aerial photographs (*top*) and difference between manual and automatic filtered DTMs (*bottom*) of the two test-areas

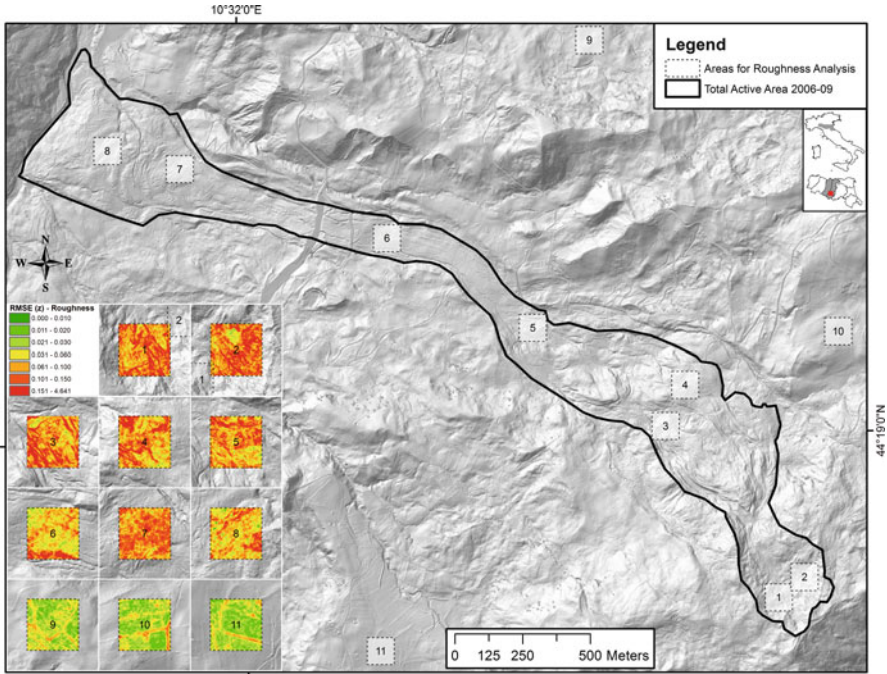


**Fig. 3.3** Map situation of the Valoria landslide showing the location of the 11 zones with different slope activity, as well as the RMSE images obtained in these zones. The frequency distributions for each zone are given in Fig. 3.4

### 3.2.2 Estimation of Surface Roughness

A valuable derivative of a DTM is the surface roughness. Different parameters quantifying roughness have been proposed in the literature, including RMSE (Root mean Square Error on height) and RMS-deviation (see Shepard et al. 2001). Two applications of roughness are shown in this paper. For the Valoria landslide (Italy), the RMSE of the surface elevation is calculated using a moving kernel, with the goal to define characteristic signatures allowing discrimination between active and stable areas. For the Avignonet and Harmallièrè landslides (Trièves area, French Alps), roughness has been estimated using the RMSD along profiles with two step-sizes.

The Valoria landslide is a complex and composite mass movement, associated with rotational and translational slides in the source area and subsequent earthflows in the track and accumulation zones (Fig. 3.3, Daehne 2011). A Lidar-based DEM, with a 1 m pixel size, was analyzed to compute roughness on specific zones with different slope activity. Point cloud filtering was applied to remove vegetation and scan line effects. Characteristic roughness signatures were calculated for eleven  $100 \times 100$  m zones with known slope activity, ranging from very disturbed areas to flat stable terrain. The locations of the 11 zones are shown in Fig. 3.3. The RMSE values

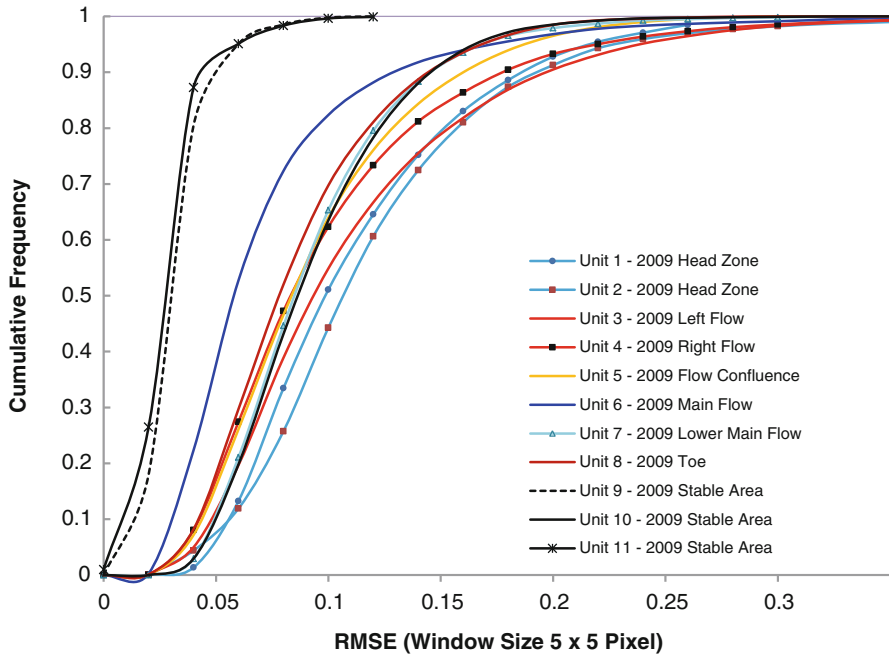


**Fig. 3.4** Cumulative frequencies of RMSE values of elevations computed for different landslide units using a  $5 \times 5$  moving window. Clearly distinguishable are stable units (*black*) with the major contributions below RMSE 0.05 with the exception of unit 10 which is slightly biased due to road embankments contained in the sample area. Head zone (*light blue*) and left flow (*red*) have a large percentage of RMSE values above 0.1. Difficulties exist to differentiate right flow, toe, flow confluence and the lower main flow. The main flow (*dark blue*) has a peak contribution from values between 0.04 and 0.08 indicating smooth terrain

of DEM elevations were computed for the different zones using a  $5 \times 5$  m moving window. A de-trending surface representing average slope conditions was applied to the background of surface roughness. The calculated RMS subsets are included in Fig. 3.3. For each zone the corresponding RMSE cumulative frequency curves are shown in Fig. 3.4. Stable areas (zones 9, 11) have RMSE values prevalently lower than 0.04, while the source and the upper track areas (zones 1–4) are characterized by a wide distribution of RMSE between 0.07 to about 0.18, with a prevalence of values above 0.06. The RMSE distributions in zones located in the lower landslide body are very similar. The smooth surface morphology of the main flow stands somewhat out (Fig. 3.4) in that RMSE values are mainly below 0.07. In conclusions, RMSE values lower than 0.04 are capable to unequivocally constrain stable areas, particularly with low vegetating coverage. Conversely, the limit of RMSE equal to 0.05 or 0.1 can be considered as a reasonable boundary for detecting rough or very rough areas, respectively, unequivocally associated to active earth slides or earth flows. In between, no definite conclusion can be drawn.

For the Avignonet and Harmalière landslides, exhibiting major differences in morphology and displacement rates (Bièvre et al. 2011), the spatial roughness distribution was calculated along profiles 10 m apart from the 2 m-resolution 2006 ALS-based DTM. Slope orientation was averaged at small-scale (SSc:  $20 \times 20$  m) and large-scale (LSc:  $200 \times 200$  m), and two height-profiles were extracted, down-slope (UD = up-down) and parallel to the slope (LR = left-right). Roughness (RMSD) was calculated along the profiles with a step-size of 2 and 20 m, at small and large scales, respectively. The four images are shown in Fig. 3.5a, b, d, e. The UD-roughness is low (dark blue) on the plateau and relatively high (red) in Harmalière, the lower part of Avignonet and the terrain along the lake. On the contrary, LR-roughness appears to be low everywhere, except along the lake. Map of Fig. 3.5c shows the difference between the UD and LR roughness maps; it reveals yellow-red areas with predominant UD-roughness and blue areas with predominant LR-roughness. Three zones are distinguished: (1) the plateau and upper part of Avignonet with no specific roughness, (2) Harmalière and lower parts of Avignonet with UD-dominated roughness and (3) the terrain below the Avignonet landslide and E of Harmalière along the lake with LR-dominated roughness. The directional roughness then appears to be a good indicator for landslide activity, revealed by down-slope roughness (created by perpendicular-to-slope scarps), while erosion, generating drainage downslope paths, is shown by roughness along contour lines. Several parts of Harmalière, as well as some regions along the lake, exhibit unpronounced (green color) directional roughness and are not easily classified.

The same maps are presented for the large-scale roughness (20 m) in the lower row of Fig. 3.5d–f. These maps are simpler, owing to the averaging effect of the large profiles (200 m) relatively to the grid-spacing of 10 m. Overall, they show the same trend as the small-scale maps, with however some differences. UD-roughness (Fig. 3.5e) includes larger areas of the upper part of Avignonet, in opposite to the small-scale case. This matches the lower activity in the upper part of Avignonet, which leads to undulated morphology with longer wavelengths. In addition, the directional roughness (Fig. 3.5f) shows LR-dominated (blue) areas along the ridges bordering the landslides. Conclusively, the directional roughness seems to be a promising parameter to classify morphology, especially for discriminating between landslide and erosion morphological patterns. Further investigation on different landslides would be needed to draw definite conclusions.

### 3.3 Combination of Ground and Airborne Data for 3D Geometry Analysis

Remote sensing techniques and geophysical prospecting methods are increasingly used to image landslide structures at the surface and at depth, respectively. Recently, ALS data were successfully used to map recent and historical landslides in gentle slope areas (Schulz 2007; van den Eeckhaut et al. 2007). Major advantages of ALS



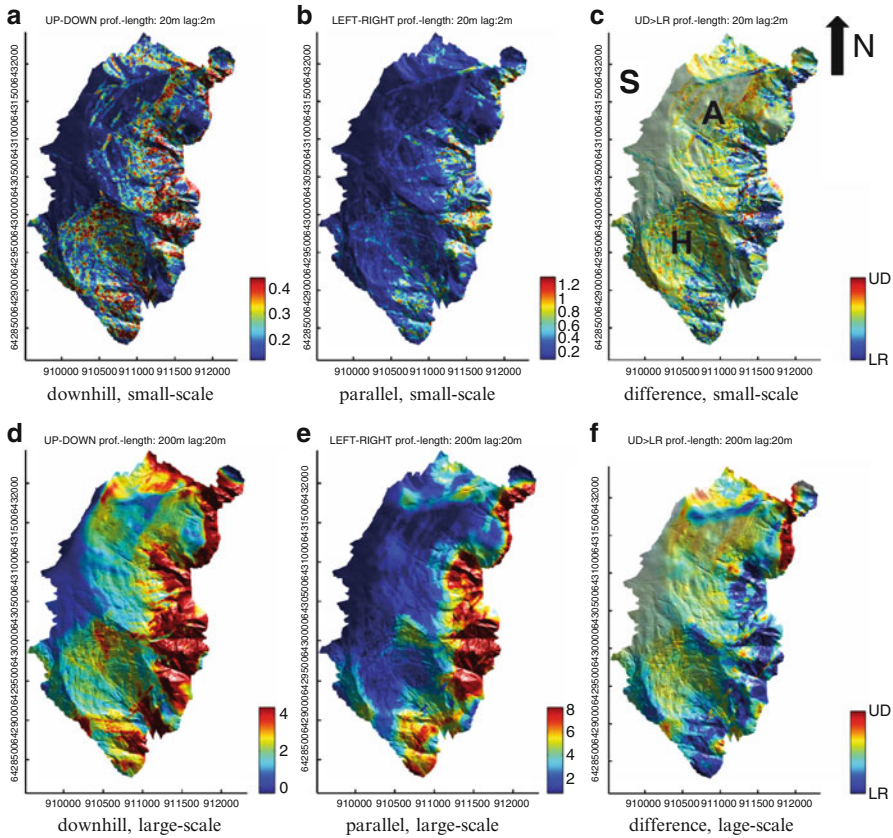


**Fig. 3.5** Small-scale (a–c) and large-scale (d–f) directional roughness calculated at locations equally distributed at every 10 m. The roughness is shown in downhill direction (a, d) and parallel to the slope (b, e). (c) and (f) present the difference between the downhill (UD) and slope-parallel (LR) roughness, meaning red areas are more rough downhill than slope-parallel and vice versa. This is meant to show the primary force of morphology alteration, landslide (red) vs. erosion (blue). The intensity of the colors in (c), (f) is the sum of the downhill and slope-parallel roughness (general roughness) in order to highlight areas with higher roughness (independent of the direction). The roughness is computed as RMSE-deviation. For small-scales the profile length is 20 m and the lag is 2 m. For large-scales, the profile-length is 200 m and the lag is 20 m. (A) Extent of the Avignonet landslide, (B) Extent of the Harmalière landslide

point cloud analysis are the flexibility and the quickness of acquisition as well as the relatively simple data processing, allowing multi-temporal Digital Elevation Models (DEM) to be generated (Oppikofer et al. 2008). In parallel, shallow geophysics has also considerably evolved with the emergence of 2D and 3D spatial imaging, allowing the study of the spatial and temporal variations inside landslides (Jongmans and Garambois 2007). Although remote sensing and geophysical techniques are

complementary for landslide imaging purposes, they have been rarely associated. Roch et al. (2006) and Deparis et al. (2008) combined remote and ground imaging techniques for determining the geometry and the 3D fracture pattern of potentially unstable cliff sites. A dense digital surface model of the rock face was measured from ALS and/or photogrammetry, while the GPR performed on the cliff allowed the discontinuity pattern inside rock mass to be obtained.

Two applications of the combination of ground and airborne data are presented. The first investigates the influence of the 3D paleotopography on the activity of two adjacent landslides in glaciolacustrine sediments located in the Trièves area (French western Alps). The second presents a data integration methodology for building 3D landslide geometry, with application to the Super-Sauze and La Valette landslides (Barcelonette Basin, France)

### ***3.3.1 Influence of Bedrock Topography on Landslide Characteristics at Large Scales***

In the Trièves Plateau, the two adjacent landslides of Avignonet and Harmalière presents major differences in morphology, displacement direction and displacement rates. GPS measurements and digital photographs reveal that the difference in kinematics between the two landslides can be tracked back to 60 years ago at least (Bièvre et al. 2011).

The Avignonet landslide is directed towards the East (N 100 E) while the Harmalière landslide is mainly oriented towards SE (Fig. 3.6a). The Harmalière landslide, which has failed catastrophically in the 1980s, is still much more active than the Avignonet landslide. A ground geophysical prospecting based on ambient noise measurements (H/V method) was performed to record the resonance frequencies at 104 locations (Fig. 3.6). The H/V technique is a single station method consisting in calculating the horizontal to vertical spectral ratios (H/V) of seismic noise records. For a single homogeneous soil horizontal layer (1D geometry) overlying bedrock, the H/V curve exhibits a peak at the resonance frequency of the soft layer (Bard 1998). Knowing the soil shear-wave velocity, the layer thickness can be calculated. The 104 measured resonance frequencies were turned into clay thicknesses. From these data and using a ALS DEM (Fig. 3.6a), a 3D map depicting the base of the clays is proposed (Fig. 3.6b). It indicates that the basement is very irregularly shaped with strong lateral E-W variations over 150 m. This map reveals the presence of a N-S ridge of hard sediments (Jurassic bedrock and/or compact alluvial layers) on the eastern side of the Avignonet landslide. This ridge disappears when approaching the Harmalière landslide and makes place to what can be interpreted like a NW-SE oriented paleo-valley of the river Drac. This ridge could act as a buttress that could mechanically prevent the Avignonet landslide from evolving as fast as the Harmalière one. Furthermore, the NW-SE paleo-valley located under the Harmalière landslide corresponds to the sliding motion direction.

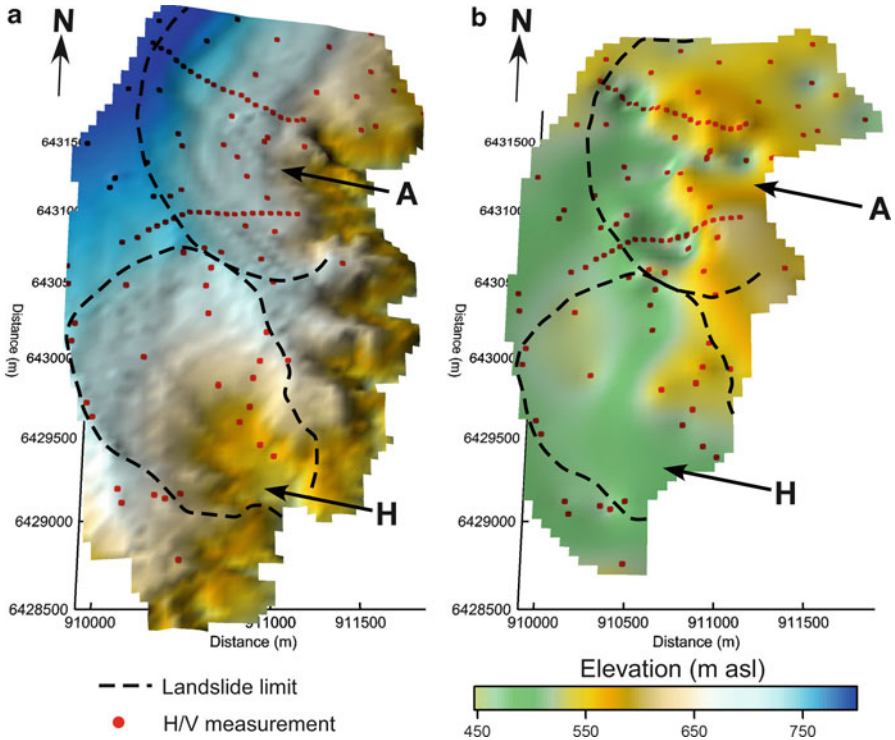


**Fig. 3.6** Avignonet and Harmalière landslides: (a) ALS-based DEM with the location of the H/V measurements, (b) Paleo-topography of the former lake Trièves in the study area. *Dashed lines* stand for Avignonet (A) and Harmalière (H) landslide boundaries

It is then proposed that the different kinematic behaviours of the landslide are partly controlled by the paleo-topographic setting of the former Trièves lake.

### 3.3.2 Methodology for 3D Geometrical Modeling at Slope Scales

The data used for landslide analysis and modeling are often numerous and acquired using different techniques, either ground-based or airborne-based. They are thus heterogeneous in terms of physical parameters, accuracy and resolutions. Therefore, a major difficulty in 3D geometrical modeling of landslide consists in the extraction of relevant information on the internal layering and on its integration in a coherent framework (Bichler et al. 2004; Regli et al. 2004; Caumon et al. 2009).

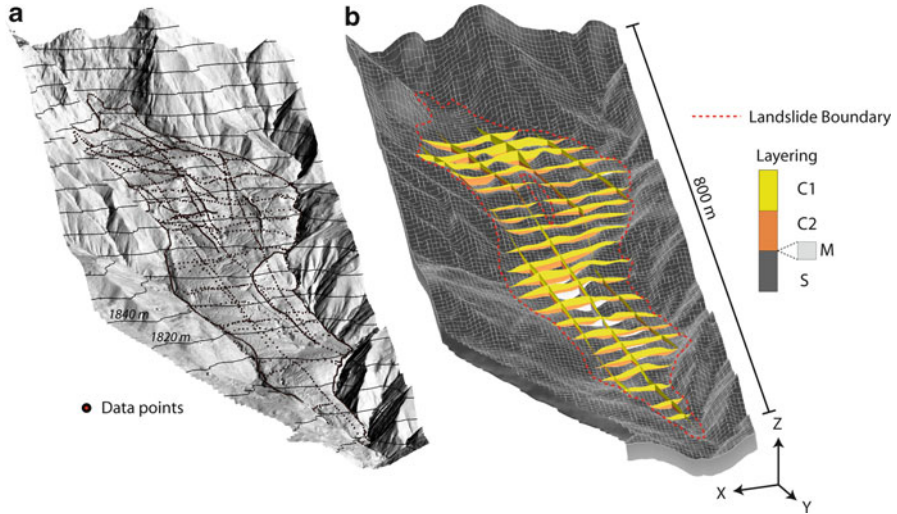


**Fig. 3.7** 3D geometrical model of the Super-Sauze landslide: (a) Location of the data points extracted from the geotechnical, geophysical and geomorphologic data, (b) 3D geometrical model illustrated through stratigraphic cross-sections interpolated with Universal Kriging. The landslide material is composed of two geotechnical layers C1 and C2 overlying the stable substratum S with some intercalation of moraine formation and torrential deposits M. (RMSE of the interfaces between C1 and C2 of 1.7 m and RMSE of the interfaces C2 and S of 2.1 m). The layers C1 and C2 have a mean thickness of 5.4 and 3.3 m. The volume of the landslide material is estimated at 560.000 m<sup>3</sup>. About 66 % of the volume corresponds to the most active layer C1

Consequently, before incorporating the data in a 3D geometrical model, several pre-processing steps are necessary: (1) to georeference the data in a common reference coordinate system, (2) to define their quality for the purpose of the modeling, and (3) to interpret (or re-interpret) the data. The problem is that, in most cases, typical data for 3D geometrical modeling are already in an interpretive digital or numerical form (e.g. maps, cross-sections) for which the uncertainty is very difficult to assess without access to the raw data.

Travelletti et al. (2011) developed a very flexible methodology applicable to any kinds of digitized data. This methodology has been successfully applied on two landslides located in the Southern French Alps: the Super-Sauze landslide developed in black marls (Fig. 3.7a) and the La Valette landslide developed in flysch formations and black marls (Fig. 3.8a). On both landslides, extensive datasets of geophysical, geotechnical and geomorphological observations are available.

In order to evaluate the quality of the data, the methodology is based on the concept of “hard data” and “soft data” initially defined by Poeter and Mckenna (1995) and Clarke (2004). “Hard data” are characterized by a high degree of reliability (e.g. explicit properties and very low uncertainties) while “soft data” are characterized by a low degree of reliability (e.g. implicit properties and higher uncertainties; Regli et al. 2004; Gallerini and De Donatis 2009). The reliability

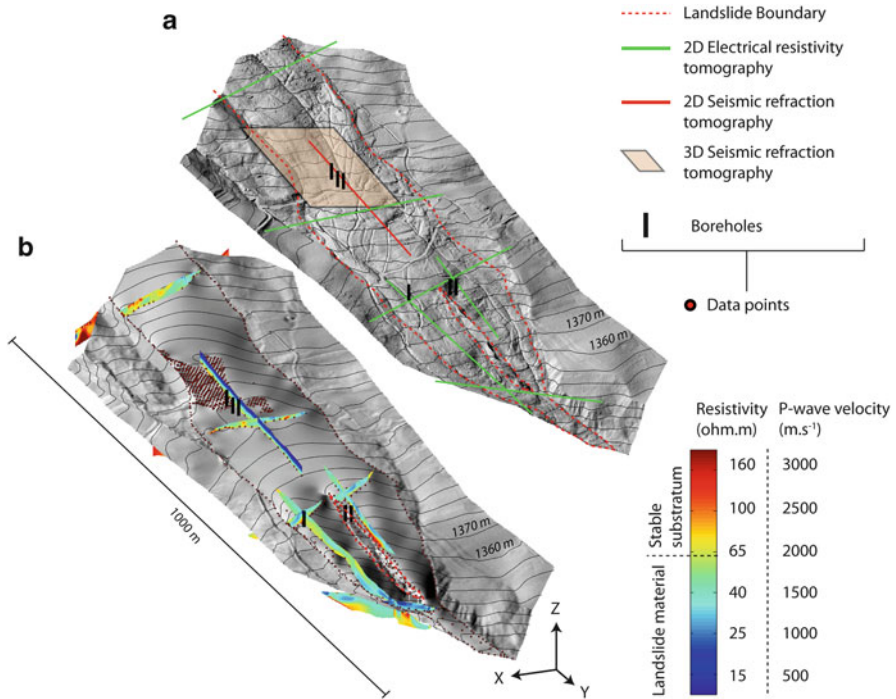


**Fig. 3.8** 3D geometrical model of the zones of transit and accumulation of the La Valette landslide. (a) Location of the geotechnical and geophysical acquisitions, (b) 3D geometrical model of the substratum topography interpolated with Universal Kriging (RMSE of 0.6 m). The data points extracted from the geophysical tomographies and from the landslide boundary are also indicated. In the zones of transit and accumulation, the depth of the landslide can reach 35 m. It represents a volume of  $2.2 \cdot 10^6 \text{ m}^3$  equivalent to 62 % of the total volume of the La Valette landslide

index depends on (i) the quality of the original data source and (ii) the number of processing steps needed to extract useful information. Travelletti et al. (2011) defined a scale of reliability index between 1 (very soft) and 4 (very hard) as follows:

1. Very soft data: The original data are noisy, inaccurate for the purpose of the analysis and with a high degree of subjectivity in the interpretation. The original data do not have accurate spatial information. They are already in an interpretative format or are derived from inaccessible raw data.
2. Soft data: The original data need several steps of processing to extract an useful geometrical information. This is usually the case for indirect data such as petrophysical properties determined with geophysical techniques at the ground surface or in boreholes. The non-uniqueness of the inverted solution and the possible decreasing resolution with depth are some drawbacks affecting the accuracy of geophysical methods (Sharma 1997; Jongmans and Garambois 2007).

3. Hard data: The original data represents generally well the geometry of the landslide, even if some ambiguities in the interpretation remain. The data have to be combined with other sources (generally geotechnical tests and geological observations) to reduce the uncertainty in the interpretation.
4. Very hard data: The original data are sufficiently accurate and allow a straightforward interpretation of the geometry without any ambiguity. The data sources are generally direct geomorphological or geological observations, borehole cores and kinematic measurements.

The coordinates of the data points used in the 3D geometrical modeling are extracted from georeferenced cross-sections and from the landslide limits in such manner that the sub-surface topography is fully preserved (Figs. 3.7a and 3.8a). A reliability index is attributed to each data point in order to associate a confidence map to the final geometrical model. This method allows one to set priority for the interpolation to the most reliable input data points. With this procedure, a null value for the reliability index is attributed to the areas unconstrained with data points. A frequent problem in data integration is caused by spatial and temporal inconsistencies among interpretive data (cross-sections or stratigraphic logs) that can be controlled and corrected with hard data located in the vicinity of the acquisition using 3D visualization tools. Temporal inconsistencies (e.g. time-dependent geometrical changes) are more difficult to detect without repetitive data acquisitions at the same location. In theory, the data should be acquired in a time short enough to avoid significant changes in the 3D geometry. In reality, these conditions are hardly ever realized because of temporal, financial and site configuration constraints. Therefore, recent data should have priority on older data. According to the quantity of available data, additional exploration might be necessary. The quality of the 3D geometrical modeling is defined by applying different interpolation techniques (Triangular Irregular Network, Inverse Distance with a weighting factor, Ordinary Kriging and Universal Kriging) and the analysis of the Root Mean Square Error (RMSE) and expert analysis (visualization of the sub-surface topography; Aguilar et al. 2005; Fisher and Tate 2006). In order to compute the RMSE, a subset of data points with a high degree of reliability is withheld from the interpolation by applying a random split-sample method (Declercq 1996). Finally, in order to obtain a geometrical model in agreement with the geological information, Travelletti et al. (2011) defined simple stratigraphic rules to avoid interferences between stratigraphic layers to provide realistic 3D geometrical models (Figs. 3.7b and 3.8b).

The 3D geometrical models of the Super-Sauze and La Valette landslides are based essentially on geophysical surveys (refraction seismic tomography, electrical resistivity tomography) and geotechnical investigations. These spatially distributed techniques were shown to be very efficient for preliminary field investigations because they provide a continuous imaging of the subsurface. However, geophysical tomographies generally display a smooth image of the sub-surface (Figs. 3.7b and 3.8b). The sub-surface appears excessively smoothed compared to the reality.

In such conditions or if no data point is available in a specific area, it is necessary to force the model to produce realistic results by adding data points coming from expert knowledge.

### **3.4 Characterization of Water Infiltration Using ERT and Temperature Monitoring**

Water infiltration plays a crucial role in landslide mechanics (Maquaire et al. 2003). Rainwater or snow melt infiltrates into the soil and recharges the groundwater system. An increase in pore water pressure reduces the internal strength of slopes and can generate instability of soil masses. However, when dealing with shale slopes, material heterogeneity strongly affects the infiltration and moisture pattern. Therefore, moisture monitoring in the shallow soil layer is of prime importance for understanding the spatial and temporal behaviour of landslides. Two applications of monitoring methods are presented here: Electrical Resistivity imaging (ERT) and high-resolution distributed sensing (DTS) using fibre-optic cables.

#### ***3.4.1 Time-Lapse Electrical Resistivity Tomography (ERT)***

Electrical resistivity of the subsoil is very sensitive to changes in water saturation and pore water salinity. Monitoring Electrical Resistivity through Tomographies (ERT) is potentially able to provide a spatial characterization of water flows within a slope (Daily et al. 1992; Binley et al. 1996; Slater et al. 2000; French and Binley 2004). Therefore, this technique is widely used to complement classical hydrological methods (Robinson et al. 2008). In complement, ERT is also particularly interesting for estimating bedrock geometry in landslide investigations when a resistivity contrast between the bedrock and the mobilized mass exists (Jongmans and Garambois 2007; Marescot et al. 2008).

In order to characterize the dynamics of water infiltration in the subsoil of heterogeneous marly landslides, rainfall experiments were carried out in 2007 and 2008 at the Laval landslide (Laval catchment, Draix, France) and at the Super-Sauze landslide (Barcelonnette Basin, France). In both study cases, the landslide material is composed of weathered Callovo-Oxfordian black marls characterized by a heterogeneous fabric of flakes and centimetric to decimetric blocks encased in a sandy-silty matrix. A multi-technique approach was set up to monitor soil deformation and soil hydrology (e.g. groundwater level measurements, soil water content monitoring, chemical tracer analysis, seismic tomography and ERT; Debieche et al. 2011).

At the Laval landslide, Travelletti et al. (2011) present an analysis of water movement based on the interpretation of ERT monitoring using a time-lapse inversion approach. The main objectives of this study were: (i) to characterize the spatial and temporal development of the water infiltration front and the subsurface flow in the soil and, (ii) to identify the time when the conditions of steady-state flow (e.g. constant water flow rate) is reached.

Six inverted models of time-lapse inversion are used to estimate the uncertainties of the resistivity values and to select the most appropriate inverted model for the hydrological interpretation. The best model has been chosen according to the RMSE of the inversion and the stability of the resistivity values in a test area where no change in resistivity is expected. The noise level due to temperature changes in the inversion process is estimated. A method for determining the time of steady-state flow conditions is proposed and this time is compared to hydrological measurements.

The experimental rain plot is located in the accumulation zone of the Laval landslide on a moderate slope gradient (ca.  $20^\circ$ ); the zone is characterized by macro-fissures at the surface which may act as possible preferential water pathways (Garel et al. 2012). The simulated rainfall was applied on an area of  $100 \text{ m}^2$  with an average intensity of  $11 \text{ mm}\cdot\text{h}^{-1}$  during 67 h and simulated using a water pump and six sprinklers located along the borders of the experimental plot. Chemical tracers (chlorure, bromure) were added to the rain water to characterize the water pathways and flow velocity. The electrical resistivity of the rain was kept constant ( $18 \text{ }\Omega\cdot\text{m} \pm 4 \text{ }\Omega\cdot\text{m}$ ) during all the experiment. A network of shallow piezometers (with varying depths of 1–4 m) was installed for water sampling and groundwater level observations. The rain experiment started with unsaturated hydrological condition in the slope material (initial saturation degree of ca. 27 %). The resistivity of the pre-event water present in the slope has an average resistivity of  $5 \text{ }\Omega\cdot\text{m} \pm 3 \text{ }\Omega\cdot\text{m}$ .

The ERT tomography is located in the central part of the experimental plot in the direction of the main slope gradient. The upstream part of the ERT line is located outside of the artificial rain in an area called ‘dry plot’. The system features an internal switch-system board for 48 electrodes with 1-m inter-electrode spacing. Data acquisition lasted approximately 15 min; an acquisition was conducted every 1–3 h. A Dipole-Dipole configuration was selected. A filtering was applied to remove all data with a measured potential lower than 5 mV. After filtering, 87 % of the original dataset was kept for the analysis. The electrical potential, the input current electrode geometry and the ERT line topography are used to compute apparent resistivity value as input to the inversion process.

To determine the effects of soil temperature on the resistivity values, soil temperature was monitored near the experimental plot along a vertical profile at different depths (–0.13, –0.30, –0.50, –0.85 m). In addition, two temperature sensors were installed inside the rain plot at –1.90 and –2.90 m in piezometers. By using the model of Campbell et al. (2002), this study shows that inverted resistivity values above 0.5 m can be very noisy due to temperature changes. However correction of temperature effects will not significantly improve the results because



the very shallow layers are generally poorly resolved in term of inverted resistivity values. Consequently inverted resistivity values above 0.5 m depth are removed from the inverted models and the consequent analysis. The apparent resistivity values were inverted using the time-lapse approach based on cross-models implemented in the RES2DINV inversion software (Loke 2006). The basic of a cross model is the use of an inverted model from a base dataset as the reference model for later datasets. Changes in subsurface resistivity are computed by using the apparent resistivity changes to ensure that changes of inverted resistivity values are only due to changes in apparent resistivity values (Loke 1999; Miller et al. 2008). Three types of cross-models were compared. The best inverted model exhibits RMSE of less than 2.2 %.

The results show a decrease of resistivity (e.g. negative anomaly) with time following directly the onset of the rain (Fig. 3.9a). The observation coincides with the development of a wetting front progressing mainly vertically during the first 10 h of the experiment. The area located downstream and outside of the rain plot is then affected by a negative anomaly showing that a lateral subsurface flow is developing. After 30 h of rain, this lateral subsurface flow may have reached the Laval stream. The evolution below the weathered clay-shales/bedrock interface is not indicated because the sensitivity is too low below it. Consequently, infiltration inside the bedrock cannot be depicted from the ERT dataset. However, regarding the lateral development of the subsurface water flow at about 20 h after the beginning of the rain, an important permeability contrast between the weathered clay-shales and the bedrock can be suspected.

Despite the difficulty of finding a reliable relationship between resistivity values and soil moisture due to the uncertainty of the inverted resistivity models (non uniqueness of the inversion, 3D effects and the insufficient range of resistivity value at the location of the soil moisture measurements), Travelletti et al. (2011) succeeded in determining the time of steady-state flows based on a noise estimation approach validated with hydrological measurements (Fig. 3.9b). On average, times of steady-state flows conditions are reached 21 h after the start of the rain. The topsoil is characterized by relatively short times varying between 5 and  $15 \pm 1$  h while deeper locations mostly reached steady-state flow conditions after  $20\text{--}28 \pm 1$  h. More time is needed for locations downstream outside the rain plot ( $30\text{--}35 \pm 5$  h) to reach steady-state conditions. This time difference between area outside and inside the rain plot strongly suggests the development of subsurface lateral flow during the rain experiment. Two preferential flow paths could be detected near the abrupt change of slope delimiting the landslide toe from the other part of the landslide body. These flow paths induce fast water infiltration until the weathered clay-shales/bedrock interface thus leading to steady-state conditions after a short time of rain experiment (ca.  $15 \pm 2$  h). These preferential flows are probably connected through the weathered clay-shales/bedrock interface. The inverse of the gradient of steady-state times is used to estimate an apparent saturated hydraulic conductivity of  $1.7 \times 10^{-4} \text{ m}\cdot\text{s}^{-1}$ . This value demonstrates the potential of the weathered soil to rapidly drain the infiltrated water. The ERT interpretations cannot explain complex hydrological behavior underlined by discrete information from direct hydrological and hydrochemical methods (e.g. isolated water at small scale

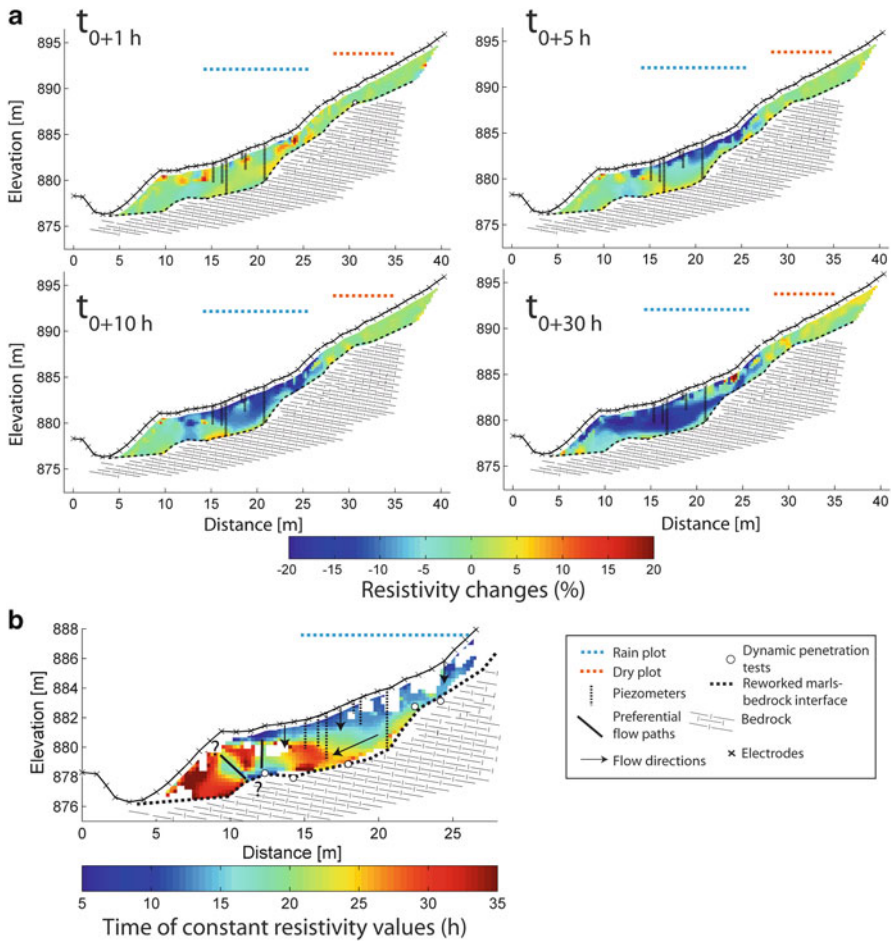


**Fig. 3.9** Results of the ERT monitoring during a rainfall experiment at the Laval landslide: (a) Resistivity changes relative to a reference inverted resistivity model before the start of the rain experiment, (b) time of constant resistivity value indicated hydrologic steady state conditions. The presence of fissure in the landslide toe allowing a rapid infiltration in depth is highlighted

with no connection with the surrounding; Garel et al. 2012). However, the main processes occurring at larger scale are highlighted. The good contrast in resistivity observed is mainly explained by the unsaturated conditions of the slope at the beginning of the experiment.

At the Super-Sauze landslide, similar experiments were realized at larger scales (rain plot areas of 1 m<sup>2</sup>) at the Super-Sauze landslide (Fig. 3.10a). In areas characterized by high density of sub-surface fissures, changes in resistivity occurred quite fast after the beginning of the rain at shallow depths and progress very slowly

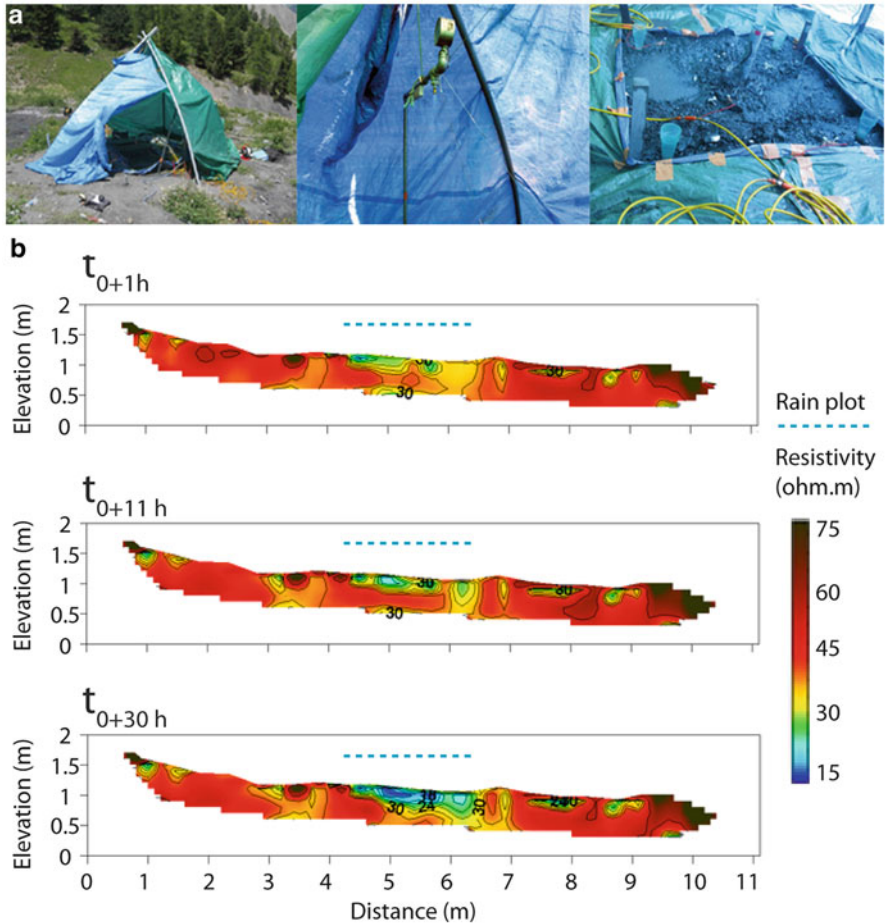


**Fig. 3.10** Large-scale rain experiment in the Super-Sauze landslide (a) presentation of the experiment rain plot: the shelter, the sprinkler and the ERT line crossing the 1-m<sup>2</sup> rain plot (b) time lapse inverted resistivity models (RMSE less than 3 %)

to greater depths (Fig. 3.10b). These observations highlight the important role of preferential flow in clayey landslide for potentially supplying in a short time surficial water to the water table.

Coupling 3D ERT at the ground surface and crossholes ERT measurements with short acquisition time would help for providing 3D interpretation of subsurface water flows and minimizing possible 3D effects. Reproducing similar rainfall experiences with different intensities and slope conditions could provide complementary and valuable information on subsurface flow development in weathered clay-shale slopes.

### 3.4.2 *High-Resolution Distributed Temperature Sensing (DTS) in the Shallow Soil*

Temperature measurements are often used in soil science to recover soil properties, including soil thermal diffusivity, which is a good indicator of changes in soil moisture conditions in time and space (Johansen 1975). Recently, high-resolution temperature measurements using fibre-optic cable have been applied in a broad range of hydrological research (Johansson and Farhadiroushan 1999; Selker et al. 2006). Distributed temperature sensing (DTS) offers the opportunity to monitor temporal and spatial temperature patterns in the soil, which is a big advantage over point temperature measurements. The method is based on the observation of back scattering and light travel time in a fibre-optic cable (for detailed description of the method and examples of hydrological applications, Selker et al. 2006). The commercially available DTS systems (e.g.: Sentinel DTS-LR<sup>®</sup> or Sensa DTS 800<sup>®</sup>) provide continuous high resolution observation (up to 1 m spatial resolution and a 60 s integration time depending on the laser configuration) over large areas (cables up to 10 km long).

One way to estimate soil thermal diffusivity from set of temperature information is the analysis of its amplitude changes within soil profile. The amplitude method (Horton et al. 1983) assumes temperature fluctuation in the soil to be sinusoidal function of time with constant period of the thermal wave in the soil and exponential decrease of its amplitude with depth. However, in the field scale measurements, application of this method gives only raw estimation of soil thermal diffusivity due to assumed simplifications. Behaegel et al. (2007) showed the capacity to estimate apparent soil thermal diffusivity by solving the heat equation for a homogenous half-space:

$$\frac{\partial T}{\partial t} = D(\theta) \cdot \frac{\partial^2 T}{\partial z^2} \quad (3.1)$$

where  $T$  is the soil temperature (K),  $t$  is the time (s),  $D$  is the apparent thermal diffusivity ( $\text{m}^2 \text{s}^{-1}$ ) and is function of soil moisture content ( $\theta$ ), and  $z$  is the depth of the soil column (m). The input data set for this estimation is air and ground temperature monitoring performed with the use of two thermistor temperature sensors installed in single soil profile. This methodology was applied to the high resolution temperature data coming from the fibre-optic cable measurements. Steele-Dunne et al. (2010) presented a feasibility study to obtain soil moisture information from passive soil DTS in a sand dune in the Netherlands. The fibre-optic cables were installed at two depths (5 and 10 cm) in a vertical profile to monitor propagation of temperature changes due to the diurnal cycle. Following Behaegel et al. (2007), Steele-Dunne et al. (2010) proposed solving Eq. 3.1 with an implicit finite difference scheme in order to optimize the apparent thermal diffusivity value to obtain the best fit between simulated and observed soil temperature within the

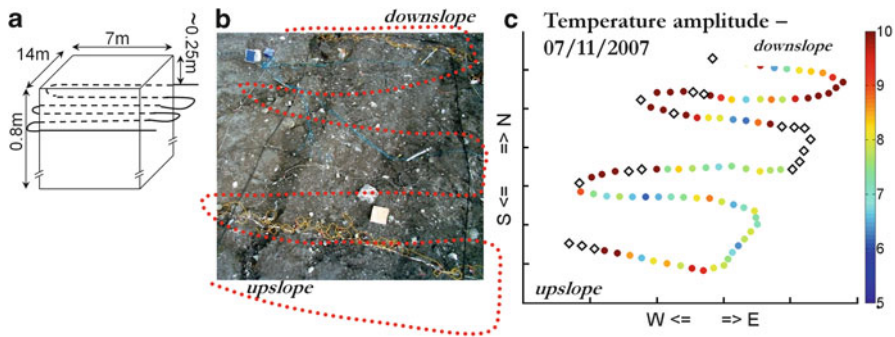


**Fig. 3.11** Setup of the high resolution Distributed Temperature Sensing: (a) Schematisation of 1st experimental set up, (b) location of the fibre-cable within experimental area, (c) example of daily soil temperature amplitude distribution within the experiment area; the rhombuses indicated the area where the cable was surfacing and measuring soil surface temperature (daily amplitude higher than 15 °C)

24-h time window. For detailed information about experimental setup, description of the optimization algorithm and results reader is referred to Steele-Dunne et al. (2010).

Based on the concepts of Steele-Dunne et al. (2010) the high resolution temperature measurements were used to test temperature as a tracer to detect spatial and temporal variation in soil thermal properties, and thus soil moisture conditions, for a clay shale material that is especially prone to landslide (Krzeminska et al. 2011). The soil temperature data were collected during two field campaigns in the black marls mudslide of Super-Sauze (France) with the use of high resolution DTS measurements. Two experimental sets were tested: 1st – using 130 m of fibre-optic cable installed at approximately 0.20 m depth, in the spiral-like shape, covering an area of approximately 100 m<sup>2</sup> (Fig. 3.11a, b), and 2nd – using two fibre-optic cables of 60 m length, installed at two depths as a straight lines, crossing three morphologically diversified sub-areas (Fig. 3.12a, b).

Figures 3.11c and 3.12c, d illustrate the qualitative analysis of observed temperature information. The differences in daily temperature amplitudes allow distinguishing between wet and dry areas at particular time (Fig. 3.11c) as low amplitude value is good indicator of the areas that might be potential wet spots. On the other hand, when looking at temperature variation in time and space (Fig. 3.12c) it is possible to get an impression about wetting and drying periods based on differences in observed temperature amplitude attenuation in time. The example of quantitative analysis of soil DTS measurements are shown in the Fig. 3.12d, e. General, higher values of apparent thermal diffusivity coincided with increases in observed soil moisture content in time and space, giving evidence for wet areas identified during cables installation, and increasing soil wetness at the end of the cables (Fig. 3.12d). Moreover, when accounting for spatial heterogeneity of soil characteristics (e.g. morphological sub-areas; Fig. 3.12b), the apparent thermal diffusivity correlated quite well with the measured soil moisture data (Fig. 3.12e).

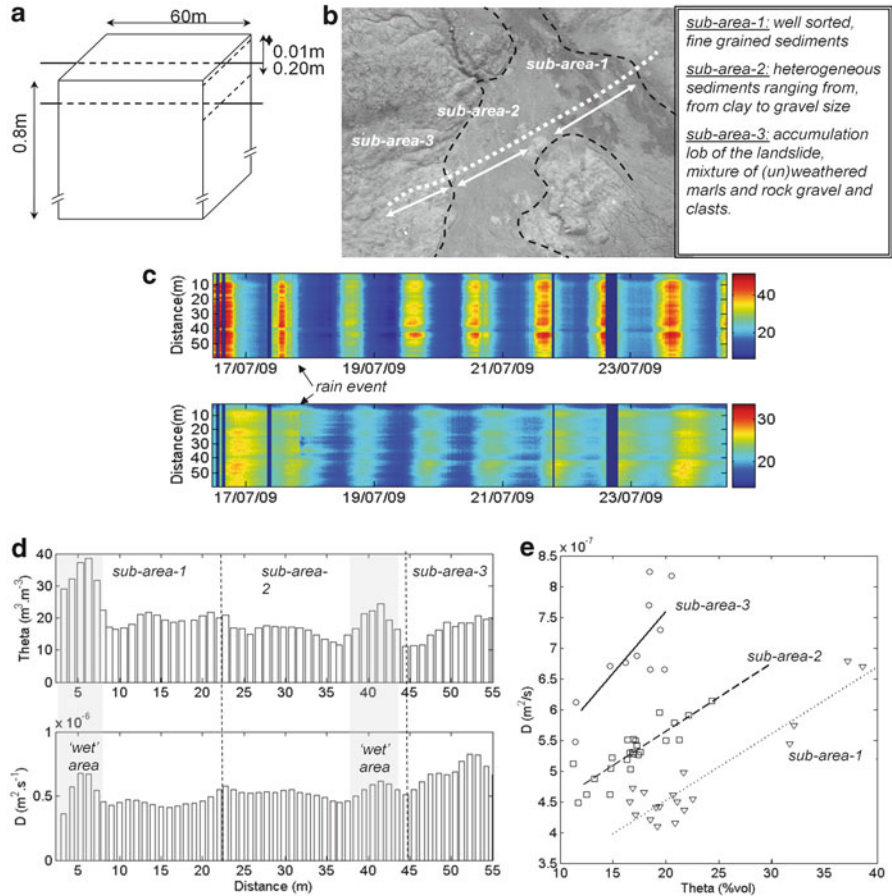


**Fig. 3.12** (a) Schematisation of 2nd experimental set up (b) location of fibre-optic cable within experimental area: the punctuate line shows the location of the fibre-optic cable and the arrows indicate morphological sub-areas.(c) Example of DTS measurements: soil surface temperature measured at 0.01 m depth (*upper bar*) and soil temperature measured at 0.20 m depth (*lower bar*), (d) Soil moisture measurements along the fibre-optic cables (*upper bar*) and estimated apparent thermal diffusivity (*lower bar*), (e) Relationship between apparent thermal diffusivity values and measured soil moisture content per sub-area

The results of Krzeminska et al. (2011) are coherent with the one presented by Steele-Dunne et al. (2010). The overall trends in estimated diffusivity values were in agreement with observed variation in soil moisture content, in spite of the fact that absolute values for thermal diffusivity were often overestimated. Moreover, both studies show that better control of the depth of sensors installation and additional measurements of the soil surface temperature resulted in a significant improvement of the calculated apparent thermal diffusivity. However, deriving soil moisture information is complicated by the uncertainty and non-uniqueness in the relationship

between thermal conductivity and soil moisture. As a stand-alone technique soil DTS and inversion method is not yet mature to give timely and effective information about soil moisture. Therefore it should be seen more as support measurements to be combined with other spatially distributed survey technique. However, giving further research attention to solve both technical and analytical complications (listed and discussed by Steele-Dunne et al. 2010) seems worthwhile since, once robust, DTS technique can provide spatial and temporal information about soil moisture stage over landslide hotspots with relatively low cost demands. In this way they could become a valuable tool to improve hazard identification, monitoring of landslide behaviour and prediction of their (re-)activation.

### 3.5 Conclusion

In the last years, landslide characterization has widely benefited from numerous and impressive developments in remote sensing, geophysics, instrumentation and data processing. The possibility of acquiring terrain information (height, displacement, depth, etc.) with high accuracy and high spatial resolution is currently opening up new ways of visualizing, modelling and interpreting these processes. These new sensors can be mounted on terrestrial, aerial and/or satellite platforms or at the ground, covering a full spectra of accuracies, resolutions, and monitoring parameters. Geophysical and geotechnical investigations can also bring additional information on subsurface processes and movements, which are essential for monitoring and early-warning systems.

In this section, recent advances for the characterization of slope morphology, structure and hydrological features are presented. Results have shown the value of complement the different techniques for a better characterization of landslide mechanisms. ALS data acquisition and processing have turned out to be promising tools for the automatic characterization of slope morphology, with the perspective of automatic detection of landslide-affected areas. Combining ALS-based DTM with ground near surface geophysical and geotechnical data allows 3D geometry of the landslide to be constructed considering data uncertainty and resolution. This is a major forward step in landslide investigation. Of major importance is also the detection of water infiltration pathways in the sliding mass, using indirect geophysical techniques such as ERT or DTS with fibre-optic cables.

### References

- Aguilar FJ, Agüera F, Aguilar MA, Carvajal F (2005) Effects of terrain morphology, sampling density and interpolation methods on grid DEM accuracy. *Photogramm Eng Remote Sens* 71:805–816
- Bard PY (1998) Microtremor measurements: a tool for site effect estimation? In: Irikura K, Kudo K, Okada H, Sasatani T (eds) *The effects of surface geology on seismic motion*. Balkema, Rotterdam, pp 1251–1279

- Behaegel M, Sailhac P, Marquis G (2007) On the use of surface and ground temperature data to recover soil water content information. *J Appl Geophys* 62:234–243
- Bichler A, Bobrowsky P, Best M, Douma M, Hunter J, Calvert T, Bunrs R (2004) Three-dimensional mapping of a landslide using a multi-geophysical approach: the Quesnel Forks landslide. *Landslides* 1(1):29–40
- Bièvre G, Kniess U, Jongmans D, Pathier E, Schwartz S, van Westen C, Villemin T, Zumbo V (2011) Paleotopographic control of landslides in lacustrine deposits (Trièves plateau, French Western Alps). *Geomorphology* 125:214–224
- Bièvre G, Jongmans D, Winiarski T, Zumbo V (2012) Application of geophysical measurements for characterizing fissures in clay landslides and understanding their role in water infiltration (Trièves area, French Alps). *Hydrol Process* 26:2128–2142
- Binley A, Henry-Poultier S, Shaw B (1996) Examination of solute transport in an undisturbed soil column using electrical resistance tomography. *Water Resour Res* 32:763–769
- Briese C, Pfeifer N, Dorninger P (2002) Applications of the robust interpolation for DTM determination. *IAPGIS XXXIV* 3A:55–61
- Campbell DI, Laybourne CE, Blair IJ (2002) Measuring peat moisture content using the dual-probe heat pulse technique. *Austr J Soil Res* 40:177–190
- Caumon G, Collon-Drouaillet P, Carlier L, de Veslud C, Sausse J, Visuer S (2009) Teacher's aide: 3D modeling of geological structures. *Math Geosci* 41(9):927–945
- Clarke SM (2004) Confidence in geological interpretation. A methodology for evaluating uncertainty in common two and three-dimensional representations of sub-surface geology. British geological survey internal report, Nottingham, IR/04/164, 29 pp
- Daehne A (2011) Innovative techniques for hazard analysis in slow-moving active earthslides-earthflows: applications to the Valoria landslide (Northern Apennines, Italy). Dissertation, Università degli Studi di Modena e Reggio Emilia, Modena
- Daily W, Ramirez A, Labrecque D, Nitao J (1992) Electrical Resistivity Tomography of vadose water movement. *Water Resour Res* 28(5):1429–1442
- Debieche TH, Bogaard TA, Marc V, Emblanch C, Krzeminska DM, Malet JP (2011) Hydrological and hydrochemical processes observed during a large-scale infiltration experiment at the Super-Sauze mudslide, France. *Hydrol Process* 26(14):2157–2170. doi:10.1002/hyp.7843
- Declercq F (1996) Interpolation methods for scattered sample data: accuracy, spatial patterns, processing time. *Cartogr Geogr Inf Syst* 23(3):128–144
- Deparis J, Fricourt B, Jongmans D, Villemin T, Effendiantz L, Mathy A (2008) Combined use of geophysical methods and remote techniques for characterizing the fracture network of a potential unstable cliff site (the 'Roche du midi', Vercors massif, France). *J Geophys Eng* 5:147–157
- Fisher PF, Tate NJ (2006) Causes and consequences of error in digital elevation models. *Prog Phys Geogr* 30(4):467–489
- French H, Binley A (2004) Snowmelt infiltration: monitoring temporal and spatial variability using time-lapse electrical resistivity. *J Hydrol* 297:174–186
- Gallerini G, De Donatis M (2009) 3D modeling using geognostic data: the case of the low valley of Foglia river (Italy). *Comput Geosci* 35:146–164
- Garel E, Marc V, Ruy S, Cognard-Planqc AL, Klotz S, Emblanch C, Simler R (2012) Large scale rainfall simulation to investigate infiltration processes in a small landslide under dry initial conditions: the Draix hillslope experiment. *Hydrol Process* 26(14):2171–2186. doi:10.1002/hyp.9273
- Horton R, Wierenga PJ, Nielsen DR (1983) Evaluation of methods for determining the apparent thermal diffusivity of soil near the surface. *Soil Sci Soc Am J* 47:25–32
- Johansen O (1975) Thermal conductivity of soils. Dissertation, University of Trondheim, Trondheim
- Johansson S, Farhadiroushan M (1999) Fibre-Optic system for temperature measurements at the Lovon dam. *Elforsk Rapport* 99:36, Stockholm, 25p



- Jongmans D, Garambois S (2007) Geophysical investigation of landslides: a review. *Bull Soc Géol France* 178(2):101–112
- Krzeminska DM, Steele-Dunne SC, Bogaard TA, Rutten MM, Sailhac P, Géraud Y (2011) High-resolution temperature observations to monitor soil thermal properties as a proxy for soil moisture condition in clay-shale landslide. *Hydrol Process* 26(14):2143–2156. doi:10.1002/hyp.7980
- Loke MH (1999) Time-lapse resistivity imaging inversion. In: Proceedings of the 5th meeting of the environmental and engineering geophysical society European section, European section, Em1, Budapest
- Loke MH (2006) RES2DINV ver. 3.55, Rapid 2D resistivity and IP inversion using the least-squares method. Software Manual, p 139
- Malet JP, Auzet AV, Maquaire O, Ambroise B, Descroix L, Esteves M, Vandervaere JP, Truchet E (2003) Investigating the influence of soil surface features on infiltration on marly hillslopes. Application to callovo-oxfordian black marls slopes in the Barcelonnette basin (Alpes-de-Haute-Provence, France). *Earth Surf Proc Land* 28(5):547–564
- Maquaire O, Malet JP, Remaître A, Locat J, Klotz S, Guillon J (2003) Instability conditions of marly hillslopes: towards landsliding or gullyng? The case of the Barcelonnette Basin, South East France. *Eng Geol* 70:109–130
- Marescot L, Monnet R, Chapellier D (2008) Resistivity and induced polarization surveys for slope instability studies in the Swiss Alps. *Eng Geol* 98:18–28
- Miller CR, Routh PS, Broster TR, McNamara JP (2008) Application of time-lapse ERT imaging to watershed characterization. *Geophysics* 73:3–17
- Oppikofer T, Jaboyedoff M, Keusen HR (2008) Collapse at the eastern Eiger flank in the Swiss Alps. *Nat Geosci* 1:531–535
- Poeter EP, Mckenna SA (1995) Reducing uncertainty associated with groundwater-flow and transport predictions. *Ground Water* 33(6):899–904
- Regli C, Rosenthaler L, Huggenberger P (2004) GEOSSAV: a simulation tool for sub-surface applications. *Comput Geosci* 30:221–238
- Robinson DA, Binley A, Crook N, Day-Lewis FD, Ferré TPA, Grauch VJS, Knight R, Knoll M, Lakshmi V, Miller R, Nyquist J, Pellerin L, Singha K, Slater L (2008) Advancing process-based watershed hydrological research using near-surface geophysics: a vision for, and review of, electrical and magnetic geophysical methods. *Hydrol Process* 22:3604–3635
- Roch KH, Chwatal E, Brückl E (2006) Potential of monitoring rock fall hazards by GPR: considering as example of the results of Salzburg. *Landslides* 3:87–94
- Schulz WH (2007) Landslide susceptibility revealed by LiDAR imagery and historical records, Seattle, Washington. *Eng Geol* 89:67–87
- Selker JS, Thevenaz L, Huwald H, Mallet A, Luxemburg W, van de Giesen N, Stejskal M, Zeman J, Westhoff M, Parlange MB (2006) Distributed fiber – optic temperature sensing for hydrologic systems. *Water Resour Res* 42:W12202. doi:10.1029/2006WR005326
- Sharma PV (1997) Environmental and engineering geophysics. Cambridge University Press, New York
- Shepard MK, Campbell BA, Bulmer MH, Farr TG, Gaddis LR, Plaut JJ (2001) The roughness of natural terrain: a planetary and remote sensing perspective. *J Geophys Res* 106:32777–32795
- Sithole G, Vosselman G (2001) Filtering of laser altimetry data using a slope adaptive filter. *Int Arch Photogramm Remote Sens Spat Info Sci* 34(3/W4):203–210
- Slater L, Binley A, Daily W, Johnson R (2000) Cross-hole electrical imaging of a controlled saline tracer injection. *J Appl Geophys* 44:85–102
- Steele-Dunne SC, Rutten MM, Krzeminska DM, Hausner M, Tyler SW, Selker JS, Bogaard TA, van de Giesen NC (2010) Feasibility of soil moisture estimation using passive distributed temperature sensing. *Water Resour Res* 46:W03534. doi:10.1029/2009WR008272
- Travelletti J, Malet JP (2012) Characterization of the 3D geometry of flow-like landslides: a methodology based on the integration of multi-source data. *Eng Geol* 128:30–48

- Travelletti J, Sailhac P, Malet JP, Grandjean G, Ponton J (2011) Hydrological response of weathered clay-shale slopes: water infiltration monitoring with time-lapse electrical resistivity tomography. *Hydrol Process* 26(14):2106–2119. doi:[10.1002/hyp.7983](https://doi.org/10.1002/hyp.7983)
- van den Eeckhaut M, Poesen J, Verstraeten G, Vanacker V, Moeyersons J, Nyssen J, Van Beek LPH, Vandekerckhove L (2007) Use of LIDAR-derived images for mapping old landslides under forest. *Earth Surf Proc Land* 32:754–769
- Zhang K, Whitman D (2005) Comparison of three algorithms for filtering airborne lidar data. *Photogramm Eng Remote Sens* 71(3):313–324